**Post-Print Version**

**Original version: http://dx.doi.org/10.1002/we.1808**

# Effects of Floating Sun Gear in a Wind Turbine's Planetary Gearbox with Geometrical Imperfections

**Amir Rasekhi Nejad[1,2], Yihan Xing[2] , Yi Guo[3] , Jonathan Keller[3], Zhen Gao[1,2], Torgeir Moan[1,2]**

[1]Norwegian Research Centre for Offshore Wind Technology (Nowitech)

[2]Centre for Ships and Ocean Structures (CeSOS)

Norwegian University of Science and Technology (NTNU)

[3]National Wind Technology Center (NWTC), National Renewable Energy Laboratory (NREL), 15013 Denver West Parkway, Golden, CO, 80401, USA

**Corresponding Author:** Amir.Nejad@ntnu.no, Tel: +47 73591546, Fax: +47 73595528

**Mailing address:** Centre for Ships and Ocean Structures (CeSOS), Norwegian University of Science and Technology (NTNU), Otto Nielsens V.10, N-7491, Trondheim, Norway

**Keywords**: wind turbine drivetrains; floating sun gear; gear misalignment; planetary gears

## Abstract

This paper addresses the effect of gear geometrical errors in wind turbine planetary gearboxes with a floating sun gear. Numerical simulations and experiments are employed throughout the study. A National Renewable Energy Laboratory 750-kW gearbox is modelled in a multibody environment and verified using the experimental data obtained from a dynamometer test. The gear geometrical errors, which are both assembly-dependent and assembly-independent, are described, and planet-pin misalignment and eccentricity are selected as the two most influential and key errors for case studies. Various load cases involving errors in the floating and nonfloating sun gear designs are simulated, and the planet-bearing reactions, gear vibrations, gear mesh loads and bearing fatigue lives are compared. All tests and simulations are performed at the rated wind speed.

For errorless gears, the nonfloating sun gear design performs better in terms of gear load variation, whereas the upwind planet bearing has more damage. In the floating sun gear scenario, the planet misalignment is neutralised by changing the sun motion pattern and the planet gear's elastic deformation. The effects of gear profile modifications are also evaluated, revealing that profile modifications such as crowning improve the effects of misalignment.

## 1- Introduction

Planetary gearboxes are widely employed in wind turbines due to their compact design and high gear ratios. The wind turbine gearboxes are often hybrid designs containing 3 stages, including planetary gears in the upwind stages and parallel gear pairs. A planetary gearbox can cost approximately half that of a conventional gearbox [1], and if it is well designed in terms of gear sizing and arrangement, its size and weight can measure approximately one-tenth of those of a conventional gearbox [2]. Planetary gearing comprises four elements: a sun gear, planets, a planet arm or carrier, and a ring gear or annulus. Various speed ratios can be obtained by arranging these elements differently in a compact design. The "epicyclic" gearbox is a general term for this group of gears, while "planetary" is commonly used for the arrangement with a stationary ring gear.

The disadvantages of planetary gearboxes come from their complexity and difficulty of access. Planetary gears are also more sensitive than parallel gears to manufacturing errors and elastic deformations in the shafts, bearings, and gearbox cage. Above all, a planetary gearbox performs the best only if equal load sharing between planets is achieved.

In principle, there are three methods of improving the load-sharing behaviour in planetary gearboxes. The first is to create flexibility in the ring gear by utilising thin rings such as the Stoeckicht design [3,4]. However, as investigated by Kahraman et al. [5], the gear tooth bending stress value is significantly higher in the gears of a flexible ring gear compared to those in a rigid ring gear.

The second method is to use flexible pins to support planet gears, as in the Hicks design concept [6], and the third and simplest method is to float the sun gear, allowing for a self-adjusting motion within the space [2,7]. Nevertheless, the floating sun gear concept is inefficient in gearboxes with more than three planets, and either a flexible pin or a flexible ring gear is needed. The reason for this requirement is based on the fundamental geometry rule stating that one surface passes through three points, so four or more planets create a redundant system with respect to the sun's orbit.

Many studies on planetary gearbox dynamic analysis are devoted to developing analytical models [8-11], with a focus on gear dynamic loads, and a few experiments are reported on wind turbine applications [12-14]. According to Musial et al. [15], most gearbox failures initiate at the bearing and do not begin through gear failures.

This paper investigates the effectiveness of a floating sun gear in a planetary wind turbine gearbox with three planets in the presence of gear geometrical imperfections. A multibody model of a 750-kW National Renewable Energy Laboratory (NREL) wind turbine, verified using the experimental results from a dynamometer test, is used throughout this study. The load cases with key geometrical errors imposed on the model are simulated and the effects on the gears and bearings are compared between floating and nonfloating sun gear designs. All comparisons are made with an input torque level of 100% obtained from the dynamometer test results, which represents the rated wind speed. An earlier work by Nejad et al. [16] shows that the wind speed near the rated speed make the greatest contributions to a gear's fatigue life.

## 2- Theory and Methodology

### 2-1- Gear Geometrical Imperfections

Manufacturing deviations, shaft, or housing deflections and clearances are inevitable in any gearbox. These deviations can influence gear performance, affect reliability, and, if they are not considered in the design, may jeopardise the gearbox system. It is therefore important that the effect of such deviations is studied and included in the numerical simulations.

In general, the main geometrical imperfections in gears can be classified into assembly-independent, such as profile deviations, and assembly-dependent, such as gear misalignment and tooth backlash.

#### 2-1-1. Tooth Profile Deviations

Although advanced computerised manufacturing techniques and high-quality controls have enabled the achievement of tolerances within narrower bands, deviation from a true, perfect involute profile is unavoidable. Tooth profile deviations are assembly-independent and caused by manufacturing machineries or workmanship. They are measured and controlled against the values specified in standards such as ISO 1328-1 [17] or American Gear Manufacturers Association [18,19] in the production line based on the desired gear quality grade, as selected by designers. Tooth deviations can occur along the pitch circle, which is referred to as pitch

deviation, throughout the profile, called profile deviation, or in line with the helix direction, called helix deviation. See ISO 1328-1 [17] for definitions and figures.

According to IEC 61400-4, wind turbine gearbox design code [20] gear quality must follow the ISO 1328 grades specified in Table 1.

Table 1: Required gear accuracy grade [20].

| **Gear type** | **Maximum accuracy as per ISO 1328-1** |
|---|---|
| External | 6 |
| Internal | 7 (8 for runout and total cumulative pitch deviation of Nitrided gears) |

The main consequences of profile imperfections are vibration and gear misalignment. Gear vibration is more sensitive to helix and profile deviations than to pitch deviation. Profile and helix deviations move the contact point position along the tooth lead and profile, causing nonuniform, time-varying load distribution on both the gear and bearing supports. Pitch error only shifts but does not change the involute profile. Based on the fundamental conjugate involute theory, the shifted involute or eccentric profile is still an involute creating smooth sinusoidal rotational error, which is not an important factor in gear vibration [2,21]. Another effect of helix deviation is axial misalignment in the assembled gears, which can also be due to the helix deviation of mating gears or assembly deviations. The latter plays a greater role than gear tooth profile deviations in generating noise or disturbing the load distribution along the facewidth.

It is important to note that the tolerance limits given by gear quality grades are measured based on unassembled, unloaded individual gears. The limits do not include the shaft, bearing, or housing structural defections. Geometrical variations in assembled gears are caused not only by gears but also by bearing imperfections and shaft tolerances. Thus, it is important to limit the deviations of assembled gears by selecting tolerance limits for each element and an appropriate gear quality level.

### 2-1-2. Misalignment, Load Sharing, and Edge Contact

Misalignment occurs when a gear's geometrical axis does not coincide with the shaft's axis. Such misalignment can be due to the position error of a gear's pinhole, the pinhole diameter,

or the elastic deformation of pins under loading. If the gear's geometrical axis is offset from the reference axis, but both are still parallel, the problem is often called eccentricity, which can be measured by a runout test as roughly half of the runout value [22].

The consequences of misaligned parallel axis gears are edge contact, vibration, and unfavourable bearing load conditions [23]. Misalignment can shift the gear pairs towards each other, filling the backlash and creating a double side flank or edge contact. In addition to this edge contact, misalignment changes the load-sharing behaviour in planetary gears, imposing an extra load on bearings [24]. According to Singh A. [7], planetary gears with a floating sun can achieve better load sharing than nonfloating systems at the presence of misalignment. This concept is examined in this paper for wind turbine gears in the gearbox case study.

#### 2-1-3. Backlash and Tooth Impact

Backlash or clearance exists in any gear system, either by design or due to manufacturing errors or wear. This backlash may induce vibro-impacts, leading to excessive vibration, noise, and dynamic loads [25].

The clearance between gear pair teeth, or backlash, is considered to be a potential source of vibration in some research papers [26,27]. The influence of clearance occurs mainly in the cases when the torque's mean value is near zero or torque reversals present in the system [28,29].

In wind turbine gearboxes, such behaviour can occur during a braking event, start-up, or fault conditions, causing impact loads on the gear teeth, irrespective of a floating or nonfloating sun. According to the experiments performed by Gu [30], the large clearance and high frequencies in a system with clearance lead to a chaotic response and a peak impact force with an amplitude two to three times greater than the applied load. The clearance used in Gu's experiment [30] is within the range of $0 \pm 0.25\,\text{mm}$, which has the same order of magnitude as the gear backlash in wind turbine drivetrains.

### 2-2- Influence of Gear Geometrical Imperfections on Gearbox Load Responses

#### 2-2-1. Effect on Gear Transmitted Load

The gear root bending stress or surface pitting, which directly affects the gear's life, is a function of the gear's transmitted or mesh load. The transmitted load $F^t$ is the resultant load from the applied input load on gear, as shown in Fig. 1. The effect of geometrical errors on $F^t$ is examined in the gearbox case study.

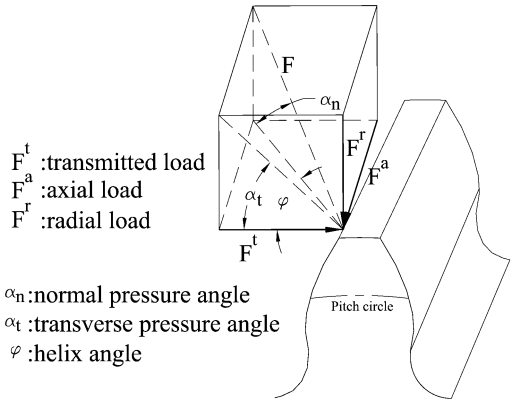


Fig. 1: Load components applied on a helical gear tooth.

### 2-2-2. Effect on Bearing Fatigue Damage

As discussed in Section 2-1, the geometrical gear error in particular misalignments affects the bearing life. The ball or roller bearings, known more generally as “anti-friction” bearings, are the most common bearings used in wind turbine gearboxes and consist of rollers, balls, races, and supporting cases. Rolling bearing life is limited by the fatigue life of the internal components and is modified by the lubricant used. Bearing design is generally based on the desired life and damage formulation established by Lundberg-Palmgren [31]:

$$P.L^{1/a} = const \qquad (1)$$

where $L$ is bearing life, $P$ the applied radial load on the bearing over a given period, $a = 3$ for ball bearing and $a = 10/3$ for the roller bearings, such as PL-A and PL-B, as in Fig. 4. Manufacturer bearing catalogues contain the basic life and load ratings established from laboratory tests. The relationship between a manufacturer’s data and the desired design parameters is expressed by:

$$L.P^a = L_{10}.C^a = const \qquad (2)$$

where $L_{10}$ is the characteristic basic rating life defined as the number of cycles that 90% of an identical group of bearings achieves, under a certain test conditions, before the fatigue damage appears. $C$ is the basic load rating and constant for a given bearing. $P$ is the dynamic equivalent radial load calculated from $P = XF_r + YF_a$, and $F_a$ and $F_r$ are the axial and radial loads on the bearing, respectively, and $X$ and $Y$ are constant factors taken from ISO 281 [32]. In the case of planet bearings, PL-A and PL-B, $X = 1.0$ and $Y = 0.0$.

Equation (2) is one form of the single SN curve formulation for high-cycle fatigue. The fatigue damage is often calculated using Palmgren-Miner's hypothesis of linear cumulative damage, given by:

$$D = \sum_i \frac{l_i}{L_i} \tag{3}$$

where $D$ is the accumulated fatigue damage for a load time history with duration $T$, $l_i$ is the number of load cycles in the time history associated with load range $P_i$, and $L_i$ comes from equation (2) and is given as $L_i = \frac{L_{10}.C^a}{P_i^a}$, which represents the number of load cycles to failure at a load range of $P_i$.

The short-term fatigue damage, $D$, can be expressed by [33,34]:

$$D = \sum_i \frac{l_i}{L_i} = \frac{\nu_{P0}.T}{L_{10}.C^a} \int_0^\infty p^a f_P(p) dp \tag{4}$$

where $f_P(p)$ is the short-term probability density function of load range $P$, $T$ is the short-term period in hours, and $\nu_{P0}$ is the number of load cycles in one hour.

Equation (4) is solved numerically; however, if $f_P(p)$ is fitted by a 2-parameter Weibull distribution, the fatigue damage can be obtained analytically by:

$$D = \frac{\nu_{P0}.T}{L_{10}.C^a} \cdot A^a \cdot \Gamma\left(1 + \frac{a}{B}\right) \tag{5}$$

where $\Gamma(\ )$ is a gamma function and $A$ and $B$ are the Weibull shape and scale parameters of the form:

$$F_P(p) = 1 - \exp\left(-\left(\frac{p}{A}\right)^B\right) \tag{6}$$

where $F_P(p)$ is the Weibull cumulative distribution function of the load range, $P$. Equation (5) is clearly based on approximation and should be used with caution. For instance, the Weibull distribution fitting can be carried by the moment method or the use of probability paper [35]. The uncertainty in distribution fitting should be reduced by having more simulation results. If 2-parameter Weibull distribution does not fit the load range, other

distributions such as generalized gamma function can also lead to an analytical fatigue damage formulation [36].

In this paper, equation (5) is used for damage comparisons; however, for design purposes, the direct approach—equation (4)—is recommended if the load range fits the 2-parameter Weibull distribution poorly. In Nejad et al. [16], the results obtained from these two equations are compared for fatigue damage in the gear tooth root.

For a given bearing in two load levels, the damage over a certain period can be compared by:

$$\frac{D_1}{D_2} = \frac{\nu_{P01} \cdot A_1^a \cdot \Gamma\left(1+\frac{a}{B_1}\right)}{\nu_{P02} \cdot A_2^a \cdot \Gamma\left(1+\frac{a}{B_2}\right)} \tag{7}$$

The $\nu_{P0}$, or the number of load cycles in one hour, can be obtained by the load duration distribution (LDD) method. The load range cycle counting for bearings is fundamentally different than shafts or structural parts in the gearbox. In every rotation, a single bearing roller experiences loads ranging from zero to a certain peak value that does not explicitly correspond to the input load fluctuations. This is because of the fact that the load range is not only a function of the external load fluctuations, but a function of the shaft rotational speed. In wind turbines, the load range for different stages should be established by taking into account both load and speed variations. Therefore, the load cycle counting method for bearings, as well as gears, is not the same as for structural components [20].

To overcome the problem with the load range and cycle counting, the LDD method, which is based on the load bins, is recommended by IEC 61400-4 [20]. More details about the LDD method for calculating fatigue damage can be found in Nejad et al. [16]. Fig. 2 illustrates the number of cycles per hour calculated by the LDD method with 95 equal bins. The graph is composed of the results for an upwind planet bearing with an errorless gear (designated as case LC0 and described in Section 5).

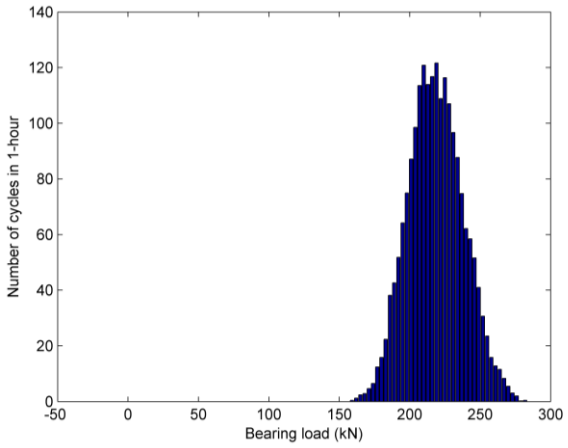


Fig. 2: Cycle counting of upwind planet bearing load.

## 3- 750-kW Gearbox Model Description

The study uses the 750-kW wind turbine provided by the Gearbox Reliability Collaborative (GRC) project at NREL [37,38]. See Table 2 for the turbine's general specifications.

Table 2: NREL 750-kW wind turbine specifications.

| | |
|---|---|
| Type | 3 blades, upwind |
| Power rating (kW) | 750 |
| Rotor dia. (m) | 48.2 |
| Rated rotor speed (rpm) | 22/15 |
| Power regulation | Stall |
| Nominal hub height (m) | 55 |
| Cut-in wind speed (m/s) | 3 |
| Rated wind speed (m/s) | 16 |
| Cut-out wind speed (m/s) | 25 |
| Design wind class | IEC Class II |
| Design life (year) | 20 |

The GRC gearbox is a three stages hybrid gearbox with two parallel and one planetary stage. The GRC drivetrain and support configuration is shown in Fig. 3. The bearings layout and gearbox topology is illustrated in Fig. 4. The floating sun gear is achieved by the spline connection of sun gear shaft to the intermediate stage. More details about the GRC gearbox model can be found in NREL's reports [37,38]. The gear specification of the planetary stage is listed in Table 3.

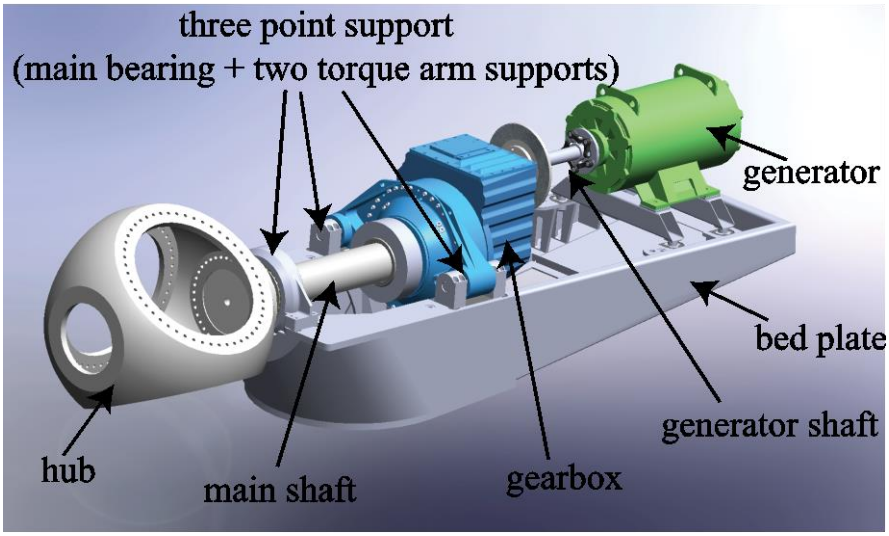


Fig. 3: 750-kW NREL drivetrain.

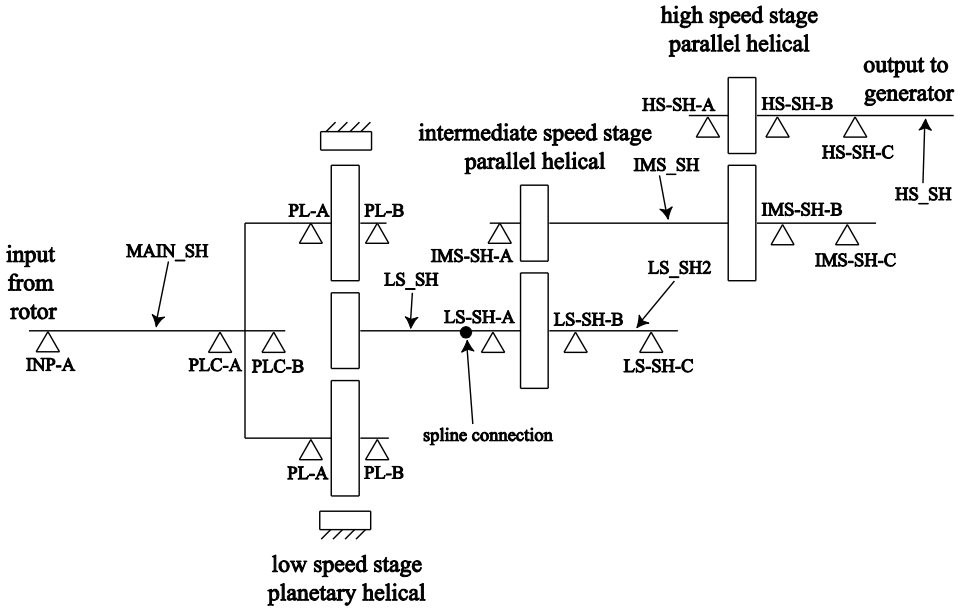


Fig. 4: 750-kW gearbox topology.

Table 3: Specification of gears in the planetary stage.

| | **Sun gear** | **Planet gear** | **Ring gear** |
|---|---|---|---|
| Normal module (mm) | 10 | 10 | 10 |
| Number of teeth | 21 | 39 | 99 |
| Normal pressure angle (°) | 20 | 20 | 20 |
| Helix angle (°) | 7.5 | 7.5 | 7.5 |
| Base diameter (mm) | 199 | 369 | 937 |
| Pitch diameter (mm) | 216 | 400 | 1016 |
| Face width (mm) | 220 | 220 | 220 |

## 4- Model Verification: Experiments and Instrumentation

A combined experimental and numerical analysis approach is used in this study. First, the global loads on the drivetrain were measured using a GRC dynamometer test bench. Next, these loads were used as inputs to a multibody drivetrain model in SIMPACK [39]. Fig. 5 shows the drivetrain model. The main shaft loads, or the forces and moments, are applied at the end of the main shaft where the rotor hub is connected.

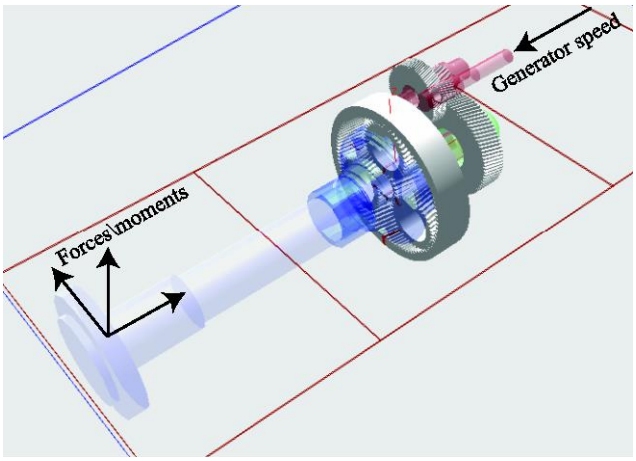


Fig. 5: Loading in the multibody model of the NREL GRC 750-kW drivetrain [44].

The NREL GRC 750-kW multibody model is built up and completed as part of the GRC project, which is verified by experiments for gearbox internal loads and employed in various earlier studies [40-47]. The bearings are modelled with linear diagonal stiffness and with clearances. More details on the gearbox and bearing modelling in multibody can be found in Xing [44]. Fig. 6 illustrates the agreement between the simulation results and measurements of the sun gear's instantaneous position under the torque applied at the rated wind speed. The X axis is downwind, parallel to the sun gear's central axis.

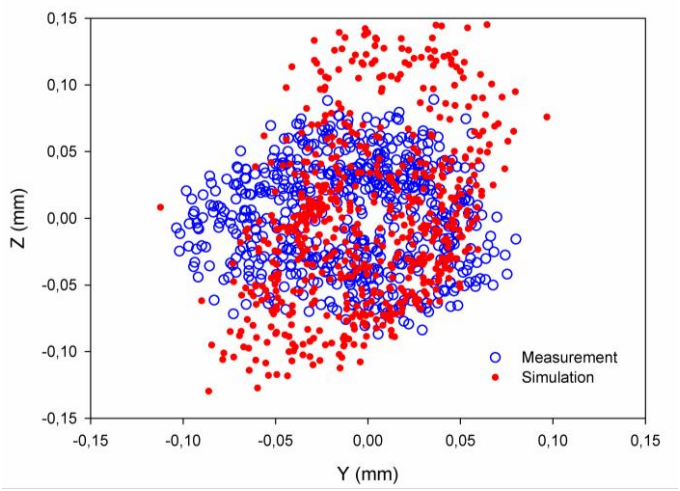


Fig. 6: Sun gear motion comparison, multibody simulation and dynamometer test measurement at rated wind speed (100% torque).

The internal measurements made of the GRC 750-kW wind turbine's gearbox include the gear tooth load distribution, main shaft torque and bending, internal component deflections and misalignments, and planet-bearing loads. A full description of the instrumentation is given in [48]. The main shaft torque and bending are measured using three sets of strain gauges in full bridge arrangements. These measurements are taken near the centre of the main shaft, between the main bearing and gearbox. The shaft torque and bending measurement serve as a reference for the input load being applied to the gearbox from the rotor side, and can also be used as the time series input for dynamic simulations. Sixty-second measurements in a steady-state, nontransient condition under 100% torque representing the rated wind speed condition are collected. The input measurement is then applied in the SIMPACK model and a simulation with time step of 0.005 is performed. The first 10 seconds are removed to avoid numerical convergence uncertainties.

For each planet bearing, three axial slots are machined into the inner diameter of the inner ring and instrumented with strain and temperature gauges. Two of the slots are located at different locations in the bearing load zone for each planet, and the third slot of each bearing is oriented 90° from the sun-planet axis. Two gauge sets in each axial slot and two bearings on each planet provide an axial distribution of four radial loads along each planet pin in addition to the total bearing loads.

Two proximity sensors are mounted on the upwind side of the planetary carrier, as shown in Fig. 7. These two sensors are positioned 90 degrees apart and measure the radial motion of the sun shaft with respect to the carrier, which suggests planetary load sharing conditions during

the operation by monitoring the sun gear's orbit motion. More information about the test and model investigation can be found in LaCava et al. [49].

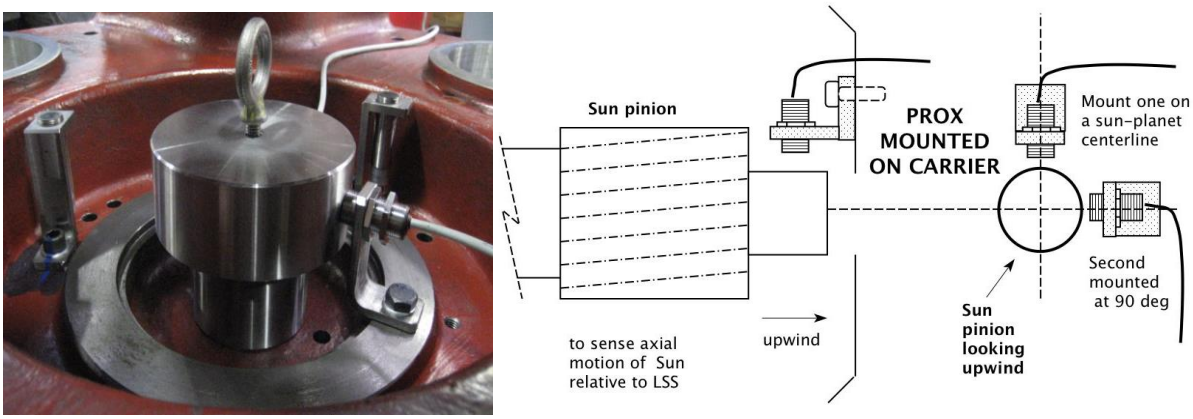


(a) (b)

Fig. 7: (a) Proximity sensors mounted on the planetary carrier, (b) relative positions of sun proximity sensors (Photo and illustration by NREL).

## 5- Case Studies

In the previous sections, the planet misalignment and eccentricity are described as two key geometrical errors in planetary gear systems. In this section, the 750-kW multibody model is studied by considering these errors with two base platforms: a floating sun gear and a nonfloating sun gear.

Table 4 describes the case studies. The planet eccentricity and misalignment are applied to planet PL1, as shown in Fig. 8 and 9. The gear tooth modifications considered for the gears include lead crowning and tip modification over a range of less than 25 microns.

Table 4: Load cases.

| Case No. | Floating Sun | Geometrical Error | Modifications |
|---|---|---|---|
| LC0 | Yes | No | Yes |
| LC1 | Yes | Yes (PL1 eccentric) | Yes |
| LC2 | Yes | Yes (PL1 misaligned) | Yes |
| LC3 | Yes | Yes (PL1 misaligned) | No |
| LC4 | No | No | Yes |
| LC5 | No | Yes (PL1 misaligned) | Yes |
| LC6 | No | Yes (PL1 misaligned) | No |

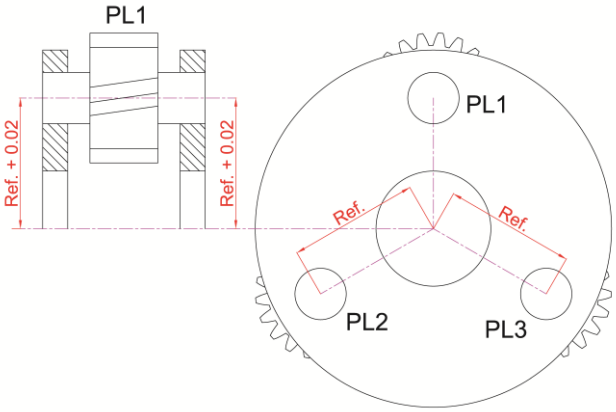


Fig. 8: PL1 eccentricity error, 0.02 mm.

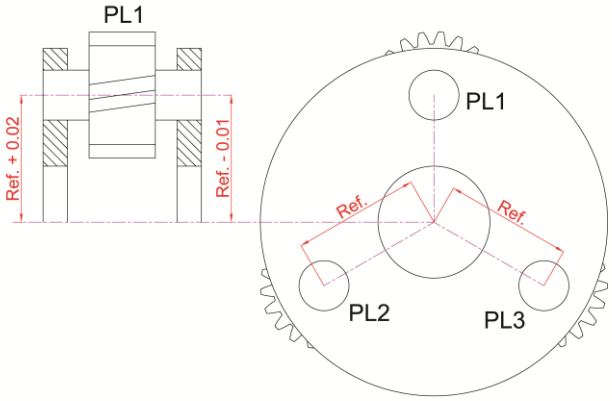


Fig. 9: PL1 misalignment error, 0.47' (minute).

The planet-bearing reactions, vibrations and force variations along the facewidth ($K_{H\beta}$) are evaluated in the case studies. $K_{H\beta}$, or the face load factor, is defined as the maximum load per unit facewidth over the average load per unit facewidth [50]. In terms of the vibrations, the sun's radial motion analysis performed by a fast Fourier transform (FFT) and the dynamic transmission error ($TE$) obtained from multibody model are used for comparison. $TE$ is defined as "the difference between the actual position of the output gear and the position it would occupy if the gear were perfectly conjugate" [2].

All of the simulation results are obtained under rated torque.

## 6- Results and Discussion

The following sections present comparative results between the floating and nonfloating sun gear designs under the load cases described in Table 4.

### 6-1- Floating Sun Gear and Errorless Planets (LC0, LC4)

The nonfloating sun gear is modelled in the multibody software by limiting the sun's motion by adding an extra stiff bearing adjacent to the sun gear. Fig. 10 illustrates the sun gear orbits with the floating and nonfloating sun designs.

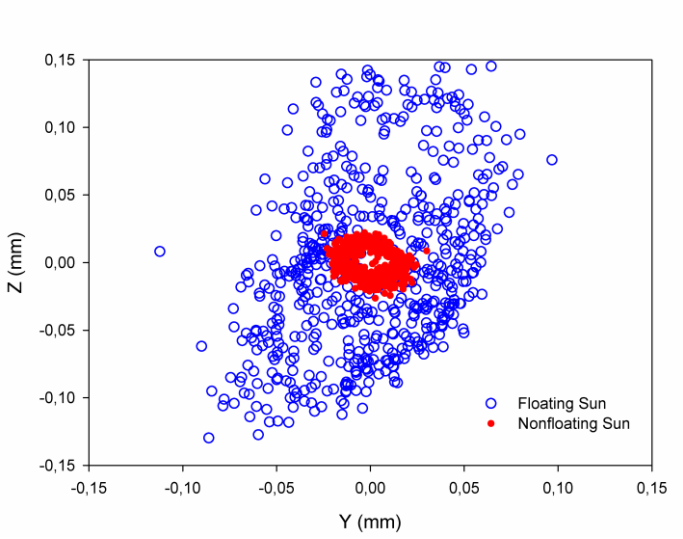


Fig. 10: Floating and nonfloating sun orbit for errorless gear (LC0 vs. LC4).

Fig. 11 compares the mean values and standard deviations of the planet-bearing reactions. Although the bearing mean values are almost unchanged, the standard deviation of the bearing reactions in the floating sun design is slightly higher than that of the nonfloating concept. A snapshot of the bearing reactions' time series is shown in Fig. 12.

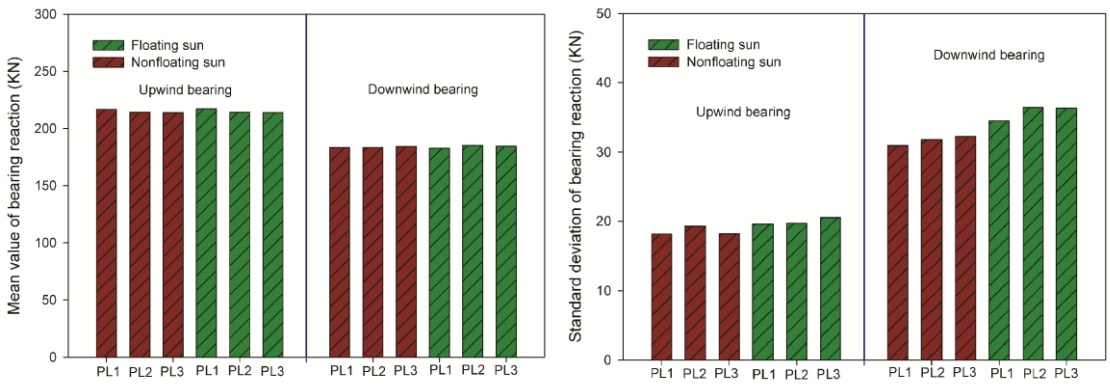


Fig. 11: Errorless gear; floating vs. nonfloating sun, mean and standard deviation of bearings reaction

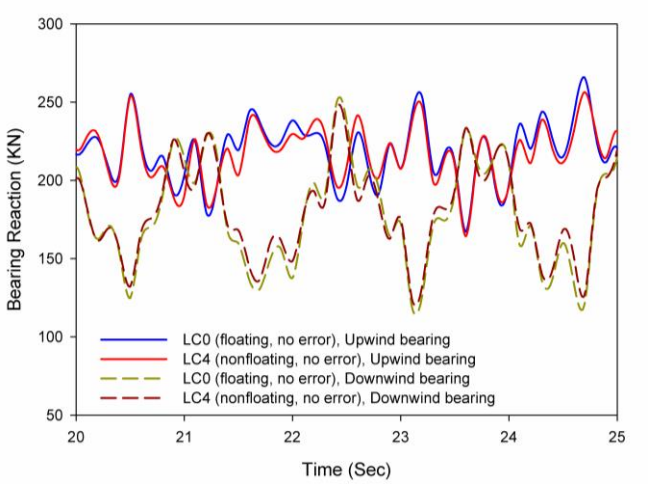


Fig. 12: Floating/nonfloating sun gear; bearing reaction comparison for PL1.

From a vibration perspective, it is found that the standard deviation of the floating sun transmission error ( *TE* ) is twice that of the nonfloating design, indicating that the noise level generated by the floating sun design is higher than that generated by the nonfloating concept. The FFT of the sun's radial motion time series, as shown in Fig. 13, also confirms the higher vibration level in the floating sun design.

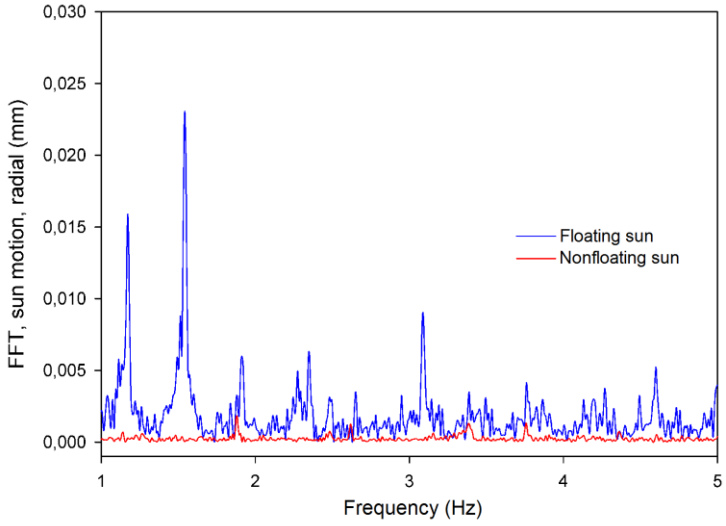


Fig. 13: Floating/nonfloating sun, FFT of sun radial in-plane motion in frequency domain without assembly error.

Based on Table 5, it appears that the standard deviation of the gear's transmitted force is slightly higher in the nonfloating sun gear design concept.

Table 5: Gear transmitted load, errorless gears, and floating vs. nonfloating sun design.

| Case No. | | Sun/PL1 | Sun/PL2 | Sun/PL3 |
|---|---|---|---|---|
| LC0 | Mean (KN) | 193.15 | 192.89 | 192.71 |
| | STD (KN) | 10.21 | 10.28 | 10.17 |
| LC4 | Mean (KN) | 193.14 | 192.94 | 192.67 |
| | STD (KN) | 11.26 | 11.21 | 11.12 |

### 6-2- Floating Sun Gear and Planet with Eccentricity (LC1)

This section considers the load case LC1, containing planet-pin eccentricity. As shown in Fig. 14, planet -pin eccentricity does not influence the sun's orbit pattern.

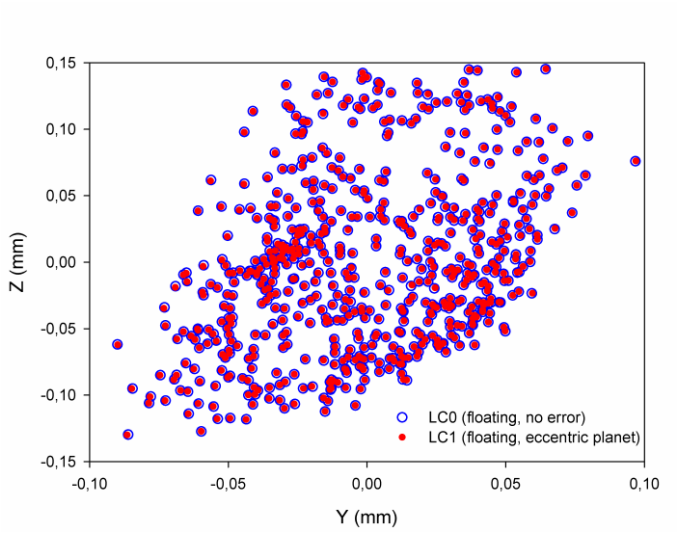


Fig. 14: Sun gear orbit in floating sun design with planet-pin eccentricity.

There are also no significant changes in the bearing reactions, as shown in Fig 15 and Table 6.

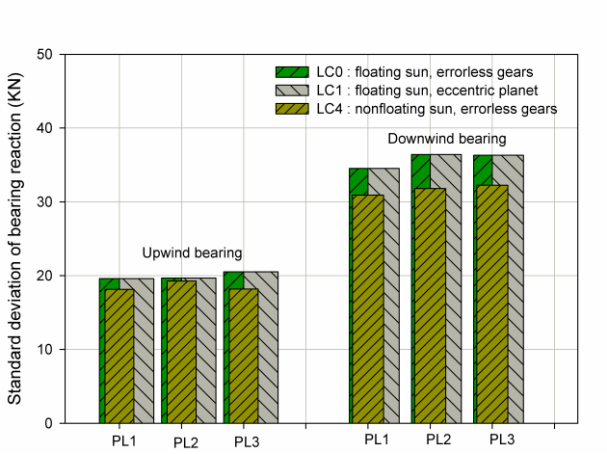


Fig. 15: Floating sun, standard deviation of bearings reaction, PL1 is eccentric.

Table 6: Bearing reaction, eccentric gear, and floating vs. nonfloating sun design.

| | | Upwind | | | Downwind | | |
|---|---|---|---|---|---|---|---|
| **Case No.** | | **PL1** | **PL2** | **PL3** | **PL1** | **PL2** | **PL3** |
| LC1 | Mean (KN) | 217.08 | 214.21 | 214.01 | 182.62 | 185.15 | 184.40 |
| | STD (KN) | 19.60 | 19.68 | 20.52 | 34.54 | 36.42 | 36.32 |
| LC4 | Mean (KN) | 216.73 | 214.14 | 213.88 | 183.38 | 183.42 | 184.40 |
| | STD (KN) | 18.16 | 19.28 | 18.18 | 30.92 | 31.80 | 32.25 |

In the floating sun design, the transmission error and transmitted gear loads with an eccentric planet are similar to the errorless gear. Gear eccentricity does not significantly affect the gearbox vibration or the load on the gears.

### 6-3- Floating Sun Gear and Planet with Misalignment (LC2, LC5)

In this case, one planet is misaligned due to the pin's position error, helix error or excessive deflection. Fig. 16 compares the orbit of the floating sun with a misaligned planet and errorless gear, and it is clear that the misalignment changes the sun motion pattern slightly.

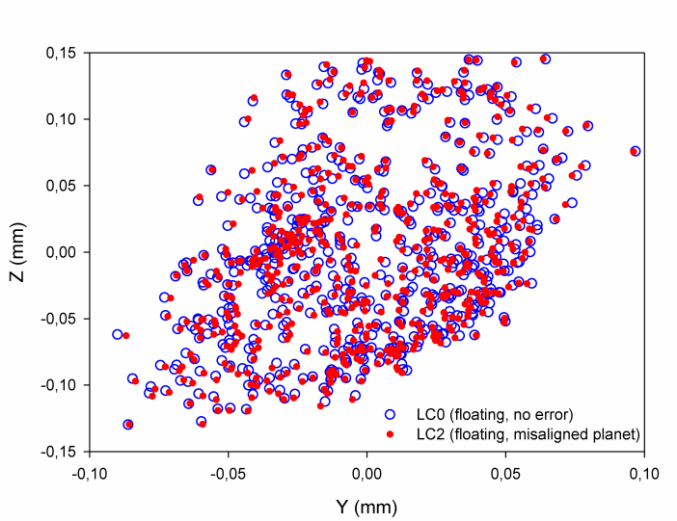


Fig. 16: Floating sun orbit for misaligned vs. errorless gear (LC2 vs. LC0).

Fig. 17 shows the standard deviations and mean values of the bearing reactions for the floating and nonfloating sun concepts.

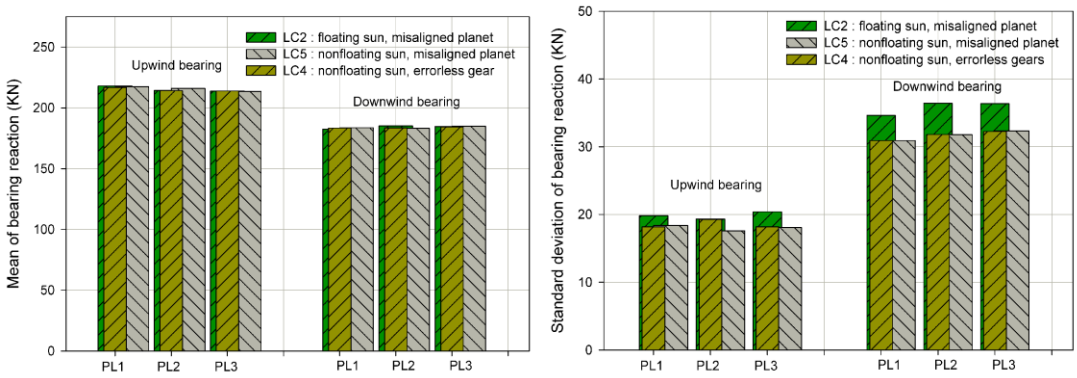


Fig. 17: Floating vs. nonfloating sun planet bearing reaction, PL1 is misaligned.

It is interesting to note that the standard deviations of the planet's bearing reactions are higher in the floating design concept with planet misalignment. The gear's transmitted force is not affected as shown in Table 7.

Table 7: Gear transmitted load, errorless vs. misaligned gear, floating sun design.

| **Case No.** | | **Sun/PL1** | **Sun/PL2** | **Sun/PL3** |
|---|---|---|---|---|
| LC0 | Mean (KN) | 193.15 | 192.89 | 192.71 |
| | STD (KN) | 10.21 | 10.28 | 10.17 |
| LC2 | Mean (KN) | 193.18 | 192.86 | 192.71 |
| | STD (KN) | 10.21 | 10.28 | 10.17 |

Shown in Fig. 18, the FFT of the sun's radial motion is compared and shows no significant difference in the vibration level of the misaligned and errorless gear in the floating design concept.

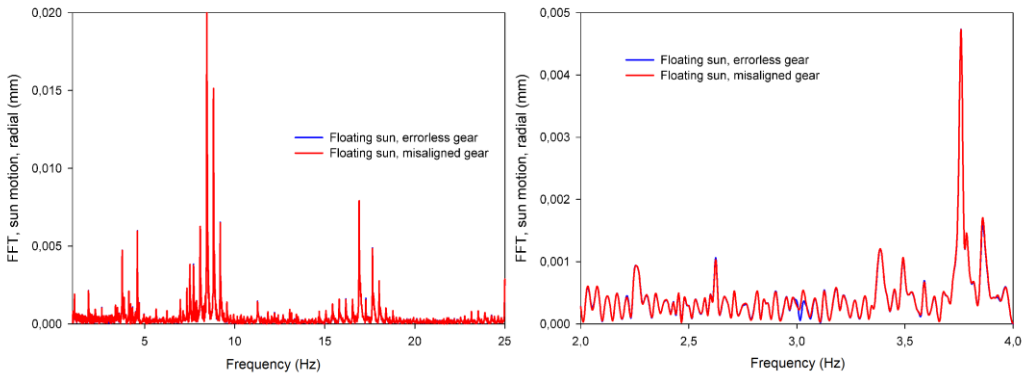


Fig. 18: (Left) Floating sun, FFT of sun radial in-plane motion in frequency domain, errorless (LC0) vs. misaligned gear (LC2); (Right) zoom for frequency 2–4 Hz.

The results of the comparison indicate that the planet misalignment is neutralised partially by the sun gear's elastic deformation (i.e., the changing sun orbit pattern) and partially by the planet deformation (i.e., increasing the bearing load).

### 6-4- Floating Sun Gear and Role of Gear Teeth Modifications

Gear lead crowning is primarily intended to improve the contact pattern under load conditions, and reduces the load variations along the facewidth, and consequently, the reactions on the bearings. The lead crowning is applied to the sun gear in this case. Fig. 19 and Fig. 20 present the influence of lead crowning on the planet bearing's standard deviation and $K_{H\beta}$ in the floating and nonfloating sun gear designs.

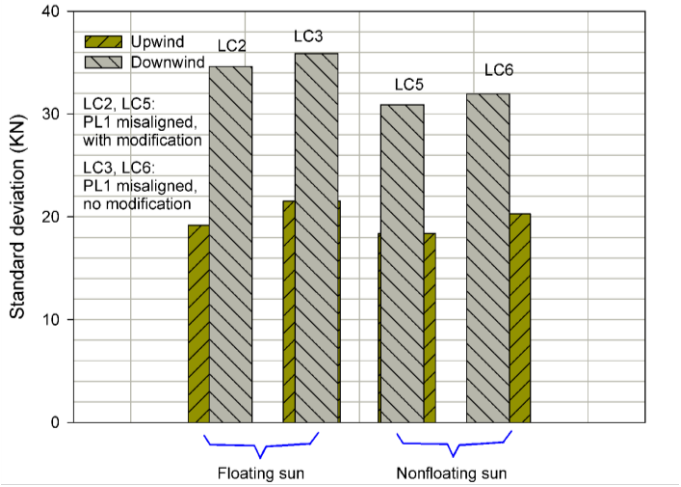


Fig. 19: Effect of gear tooth modification (lead crowning) on the reactions of the planet bearings.

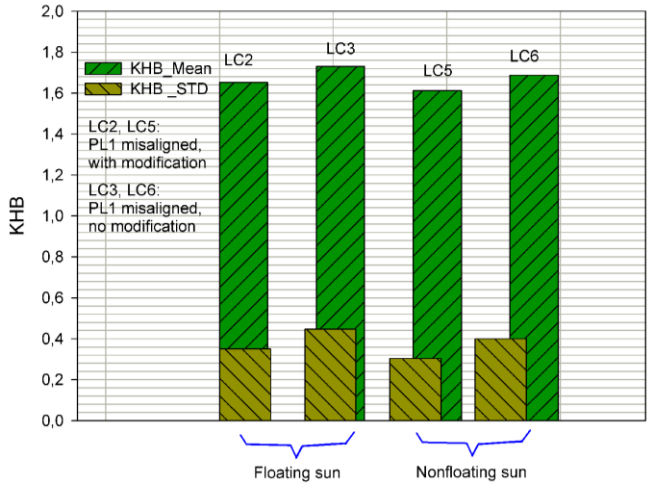


Fig. 20: Effect of gear tooth modification (lead crowning) on planet load distribution factor ($K_{H\beta}$).

In both the floating or nonfloating sun gear designs, the standard deviations of the bearing reactions and face load distribution factors are lower for the sun gear with the lead crowning, regardless of case (errorless or misaligned planet).

### 6-5- Planet-Bearing Fatigue Damage Comparison

The short-term upwind and downwind bearing damage at the rated torque level for floating and nonfloating sun design are compared by equation (7). Table 8 presents the Weibull distribution parameters of the bearing load, as described by equation (6). The $v_{P0}$, or the number of load cycles in one hour is obtained from LDD method as 2031.4 cycles for all cases.

Table 8: Weibull distribution parameters for the bearing load range.

| | **Upwind** | | **Downwind** | |
|---|---|---|---|---|
| | $A$ (kN) | $B$ | $A$ (kN) | $B$ |
| LC0 | 235.89 | 14.56 | 202.08 | 7.98 |
| LC1 | 235.90 | 14.51 | 202.09 | 7.98 |
| LC2 | 236.73 | 15.04 | 202.29 | 7.69 |
| LC4 | 235.88 | 15.31 | 200.63 | 10.19 |
| LC5 | 237.32 | 14.62 | 201.37 | 9.29 |

A comparison of the bearing damage results is shown in Table 9.

Table 9: Comparison of the PL1 bearings' short-term fatigue damage.

| $\frac{D_1}{D_2}$ | **Description** | **Upwind** | **Downwind** |
|---|---|---|---|
| $\frac{D_{LC4}}{D_{LC0}}$ | Nonfloating sun errorless gears (LC4) / Floating sun errorless gears (LC0) | 1.00 | 0.98 |
| $\frac{D_{LC2}}{D_{LC0}}$ | Floating sun misaligned planet (LC2) / Floating sun errorless gears (LC0) | 1.01 | 1.00 |
| $\frac{D_{LC1}}{D_{LC0}}$ | Floating sun eccentric planet (LC1) / Floating sun errorless gears (LC0) | 1.00 | 1.00 |
| $\frac{D_{LC5}}{D_{LC0}}$ | Nonfloating sun misaligned planet (LC5) / Floating sun errorless gears (LC0) | 1.02 | 0.99 |

Table (9) illustrates the damage in the bearings, with higher damage indicating lower life. An immediate finding from the comparison results is that the floating sun design improves the bearing life compared to the nonfloating concept in the case of gear misalignment. It also appears that upwind bearings have a lower life when misalignment exists.

Research by August and Kasuba [8] concludes that the nonfloating sun gear arrangement generally performs better than a floating sun gear for errorless gears. Their work and many other studies [7,10,11,51] evaluates the dynamic loads on gears without considering bearings. From a gear perspective, as shown in Section 6-1, the standard deviation of gear loads is slightly higher in the nonfloating sun gear design concept than in the floating concept, which confirms the conclusion made by August and Kasuba [8]. For bearings, however, it appears that the upwind bearing has a lower life in both design concepts. Furthermore, the results in Table 9 show that planet-pin eccentricity does not affect bearing life in floating design.

## 7- Conclusions

This paper investigates the influences of key gear geometrical errors, planet gear eccentricity, and misalignment on a wind turbine's planetary gearbox performance and the role of the floating sun design. A detailed multibody model of an NREL 750-kW turbine is employed and verified using experimental data from a dynamometer test. The results from this multibody model simulation study agree with the outcomes of the analytical models created by Singh [7,11], Gu and Velex [10], and Ligata and Kahraman [51] and exemplified by smaller planetary gearboxes. Moreover, the unequal loading between the upwind and downwind bearings found in this study corresponds with the previous works by LaCava et al. [14], [42]. However, the bearing damage investigation is not evaluated in earlier research. It is found that the upwind planet bearing has a lower life than the downwind bearing in both the floating and nonfloating design concepts. The comparisons are conducted at rated wind speed.

The results based on the analyzed case studies can be summarised as follows:

- For errorless gears, the nonfloating sun design has lower dynamic loads on gears than the floating sun design.
- The upwind and downwind planet bearing lives are unequal in the nonfloating sun design. The upwind bearing has higher risks of fatigue damage.

- In the floating sun gear design, planet misalignment is neutralised partially by the sun gear's elastic deformation (i.e., a changing sun orbit pattern) and partially by planet deformation (i.e., increasing the bearing load).
- Planet eccentricity does not affect the sun's orbit or the planet's bearing load in the floating sun design.
- Gear teeth modifications, such as lead crowning, improve the effects of misalignment.
- The floating sun design causes higher noise and vibrations than the nonfloating design.

Current study is based on a three-planet wind turbine gearbox. The sensitivity of the gearbox to manufacturing errors and deformations will increase in larger gearboxes with a larger number of planets. Therefore, future work will be devoted to investigating gearboxes with a larger number of planets as well as to evaluate the effect of nontorque loading on gearboxes.

**Acknowledgements**

The authors wish to acknowledge the financial support provided by the Research Council of Norway through the Norwegian Research Centre for Offshore Wind Technology (Nowitech) and the Centre for Ships and Ocean Structures (CeSOS). The gearbox, wind turbine model, and test results were gratefully obtained from the Gearbox Reliability Collaborative (GRC) project at the National Renewable Energy Laboratory in Golden, Colorado, USA. The GRC initiative is funded by the US Department of Energy Wind and Water Power Technologies Office.

**References**

[1] Hau E. Wind Turbines Fundamentals, Technologies, Application, Economics, 2nd edition, 2006, Springer, Germany.

[2] Smith J. D. Gear noise and vibration, second edition, 2003, Marcel Dekker Inc.

[3] Stoeckicht, W. G. "STOECKICHT," U.S. Patent No. 2,737,064. 6 Mar. 1956.

[4] Ziegler P., Eberhard P., Bernhard S. Simulation of impacts in geartrains using different approaches, Archive of applied mechanics; Springer, 2006: 76, 537-548.

[5] Kahraman A., Kharazi A. A., Umrani M. A deformable body dynamic analysis of planetary gears with thin rims, Journal of sound and vibration; 2003: 262, 752-768.

[6] Cunliffe F., Hicks R. Optimised gearbox design for modern offshore wind turbines, Proceeding of European Wind Energy Association Annual Conference 2004 (AWEC 2004), London, UK.

[7] Singh A. Load sharing behaviour in epicyclic gears: physical explanation and generalized formulation, Mechanism and Machine Theory; 2010: 45, 511-530.
[8] August R., Kasuba, R. Torsional vibrations and dynamic loads in a basic planetary gear system. ASME, Transactions, Journal of Vibration, Acoustics, Stress, and Reliability in Design, 1986: 108, 348-353.
[9] August R., Kasuba R., Frater J. L., Pintz A. Dynamics of planetary gear trains, NASA CR 3793, June 1984.
[10] Gu X., Velex P. On the dynamic simulation of eccentricity errors in planetary gears, Mechanism and Machine Theory; 2013,61: 14-29.
[11] Singh A. Epicyclic load sharing map - development and validation; Mechanism and Machine Theory: 2011, 46: 632-646.
[12] Helsen J., Vanhollebeke F., Marrant B., Vandepitte D., Desmet W. Multibody modelling of varying complexity for modal behaviour analysis of wind turbine gearboxes, Renewable Energy; 2011: 36, 3098-3113.
[13] Crowther A., Ramakrishnan V., Zaidi N. A., Halse C., Sources of time-varying contact stress and misalignments in wind turbine planetary sets, Wind Energy; 2011: 14, 637-651.
[14] LaCava W., Xing Y., Marks C., Guo Y., Moan T., Three-dimensional bearing load share behaviour in the planetary stage of a wind turbine gearbox, IET Renewable Power Generation; 2013: 7(4), 359-369.
[15] Musial W., Butterfield S., McNiff B. Improving wind turbine gearbox reliability. Proceeding of European Wind Energy Annual Conference, EWEA 2007, 7-10 May, Milan, Italy.
[16] Nejad A. R., Gao Z., Moan T. On long-term fatigue damage and reliability analysis of gears under wind loads in offshore wind turbine drivetrains, International Journal of Fatigue; 2014: 61, 116-128.
[17] ISO 1328-1, Cylindrical gears – ISO system of accuracy – part 1: definitions and allowable values of deviations relevant to corresponding flanks of gear teeth, first edition, 1995.
[18] American Gear Manufacturers Association, AGMA 2015/915-1-A02, Accuracy Classification System – Tangential Measurement Tolerance Tables for Cylindrical Gears, 2002.
[19] American Gear Manufacturers Association, AGMA 915-3-A99, Inspection Practices – Gear Blanks, Shaft Centre Distance and Parallelism, 1999.

[20] International Electrotechnical Commission, IEC 61400-4: Wind turbines – Part 4: Standard for design and specification of gearboxes, 2012.
[21] White R. Exploration of a strategy for reducing gear noise in planetary transmissions and evaluation of laser vibrometry as a means for measuring transmission error, PhD dissertation, Department of Mechanical and Aerospace Engineering, Case Western Reserve University, USA, 2006.
[22] ISO TR 10064-2, Code of inspection practice – Part 2: Inspection related to radial composite deviations, runout, tooth thickness and backlash, first edition, 1995.
[23] Litvin F. L., Perez I. G., Fuentes A., Hayasaka K., Yukishima K. Topology of modified surfaces of involute helical gears with line contacts developed for improvement of bearing contact, reduction of transmission errors, and stress analysis, Mathematical and Computer Modelling; 2005 :42, 1063-1078.
[24] Nejad A. R., Moan T. Effect of geometrical imperfections of gears in large offshore wind turbine gear trains: 0.6-10 MW case studies, European Annual Wind Energy Conference (EWEA), Copenhagen, 2012.
[25] Singh R., Xie H., Comparin R. J. Analysis of automotive neutral gear rattle, Journal of sound and vibration; 1989: 131 (2), 177-196.
[26] Mo. E, Naess A. Non-smooth dynamics by path integration – an example of chaotic response of a meshing gear pair, Computational Stochastic Mechanics CSM-5, 2007.
[27] Naess A., Kolness F.E., Mo E. Stochastic spur gear dynamics by numerical path integration, Journal of sound and vibration; 2007: 302: 936-950.
[28] Guo Y., Keller J., LaCava W., Combined effects of gravity, bending moment, bearing clearance, and input torque on wind turbine planetary gear load sharing, NREL report no. NREL/CP-5000-55968, National Renewable Energy Laboratory, USA, Sep. 2012.
[29] Guo Y., Keller J., Parker R., Dynamic analysis of wind turbine planetary gears using an extended harmonic balance approach, NREL report no. NREL/CP-5000-55355, National Renewable Energy Laboratory, USA, Sep. 2012.
[30] Gu P., Dubowsky S. Proceeding of the ninth world congress of the theory of machines and mechanism, Spt. 1-3, 1995, Milan, Italy.
[31] Lundberg G., Palmgren A. Dynamic capacity of rolling bearings, Acta Polytechnica Mechanical Engineering Series 1952; 2: 5–32.
[32] ISO 281, Rolling bearings - Dynamic load ratings and rating life, 2007.

[33] Naess A., Moan T. Stochastic dynamics of marine structures, Cambridge University Press, 2012.
[34] Almar-Naess A. Fatigue handbook offshore steel structures, Tapir, Norway, 1985.
[35] Ang A., Tang W., Probability concepts in engineering, John Wiley & Sons, 2007.
[36] Dong W., Moan T., Gao Z. Long-term fatigue analysis of multi-planar tubular joints for jacket-type offshore wind turbine in time domain. Engineering Structures; 2011:33, 2002-2014.
[37] Oyague F., Butterfield C. P., Sheng S. Gearbox Reliability Collaborative Analysis Round Robin, Technical Report, National Renewable Energy Laboratory, NREL/CP-500-45325, 2009.
[38] Link H., LaCava W., Van Dam J., McNiff B., Sheng S., Wallen R., McDade M., Lambert S., Butterfield S., Oyague F. Gearbox reliability collaborative project report: findings from phase 1 and phase 2. Technical Report, National Renewable Energy Laboratory, 2011.
[39] A multibody simulation package from SIMPACK AG, www.simpack.com.
[40] Oyague F. Gearbox modelling and load simulation of a baseline 750-kW wind turbine using state-of-the-art simulation codes, Technical Report, National Renewable Energy Laboratory, NREL/TP-500-41160, 2009.
[41] Xing Y., Moan T. Multi-body modelling and analysis of a planet carrier in a wind turbine gearbox, Wind Energy; 2013: 16, 1067-1089 (DOI: 10.1002/we.1540).
[42] LaCava W., Xing Y., Guo Y., Moan T. Determining wind turbine gearbox complexity using measurement validation and cost comparison, European Wind Energy Annual Conference (EWEA 2012), Copenhagen, Denmark.
[43] Dong W., Xing Y., Moan T., Gao Z. Time domain-based gear contact fatigue analysis of a wind turbine drivetrain under dynamic conditions, International Journal of Fatigue; 2013: 48, 133-146.
[44] Xing Y. Modelling and analysis of the gearbox in a floating spar-type wind turbine, Ph.D. thesis, Department of Marine Technology, Norwegian University of Science and Technology, 2013.
[45] Nejad A. R., Odgaard P. F., Gao Z., Moan T. A prognostic method for fault detection in wind turbine drivetrains. Engineering Failure Analysis, 2014; 42: 324-336.
[46] Nejad A. R., Gao Z., Moan T. Fatigue Reliability-Based Inspection and Maintenance Planning of Gearbox Components in Wind Turbine Drivetrains. Energy Procedia, 2014; 53: 248-257.

[47] Odgaard P. F., Nejad A. R. Frequency Based Wind Turbine Gearbox Fault Detection Applied to a 750 Kw Wind Turbine, Proceeding of IEEE Multi-conference on Systems and Control, October 8-10, 2014, Antibes, France.
[48] Link H., Keller J., Guo Y., McNiff B. Gearbox Reliability Collaborative Phase 3 Gearbox 2 Test Plan, Technical Report, National Renewable Energy Laboratory, NREL Report No. TP-5000-58190, 2013.
[49] LaCava W., Keller J., McNiff B. Gearbox Reliability Collaborative: test and model investigation of sun orbit and planet load share in a wind turbine gearbox, National Renewable Energy Laboratory, NREL/CP-5000-54618, 2012.
[50] ISO 6336-1, Calculation of load capacity of spur and helical gears – Part 1: basic principles, introduction and general influence factors, 2006.
[51] Ligata H., Kahraman A., Singh A. An experimental study of the influence of manufacturing errors on the planetary gear stresses and planet load sharing, ASME Journal of Mechanical Design; 2008: 130,1-9.